Journal of Power Sources 396 (2018) 102–108

Contents lists available at ScienceDirect

Journal of Power Sources

journal homepage: www.elsevier.com/locate/jpowsour

Fabrication of high-energy hybrid capacitors by using carbon-sulfur composite as promising cathodes

Bin He, An-Hui Lu, Fei Cheng, Xiao-Fei Yu, Dong Yan, Wen-Cui Li*

School of Chemical Engineering, State Key Laboratory of Fine Chemicals, Dalian University of Technology, Dalian 116024, PR China

HIGHLIGHTS

- Hybrid capacitor is fabricated with porous carbon-sulfur as cathode materials.
- The hybrid device displays high energy density of 125.3 Wh kg^{-1} at 17350 W kg^{-1}.
- The application of sulfur is extended to a new field.

ARTICLE INFO

Keywords:
Hybrid capacitors
Carbon-sulfur cathode
Hard carbon
High energy density

ABSTRACT

The full realization of the high energy density concept in current hybrid capacitors is still a challenge due to the huge difference in specific capacity and reaction kinetics of the commonly used cathode and anode materials. Herein, for the first time, the carbon-sulfur composite is proposed as the high-capacity cathode for hybrid capacitors to achieve a high energy density. The as-prepared carbon-sulfur composite delivers a high specific capacity of 212.2 mAh g^{-1} (424.4 F g^{-1}) at 4 A g^{-1}, which is much higher than that of the pure carbon cathode. Additionally, the kinetics gap between cathode and anode is narrowed by using carbon-sulfur composite as the cathode. As a result, the carbon-sulfur composite based hybrid capacitor delivers a high energy density of 258.4 Wh kg^{-1} at 995 W kg^{-1}. Even at high power density of 17350 W kg^{-1}, the energy density can still remain 125.3 Wh kg^{-1}. This study provides an alternative approach for designing hybrid capacitors with both high energy and power density by using carbon-sulfur composite as the cathode, and also paves a way to extend the application of sulfur to a new field for taking its advantages of high-capacity, environmental friendliness, low-cost.

1. Introduction

The ever-increasing demand for energy storage systems with high energy and power density applied in the field of portable electronic devices and electric vehicles has sparked the intensive research in hybrid capacitors due to its combination of the merits of both high-energy lithium-ion batteries (LIBs) and high-power supercapacitors (SCs) to bridge the gap between them [1–5]. Up to now, activated carbon (AC) is still unbeatable cathode material for hybrid capacitors because it allows hybrid capacitors to be operated at a high voltage [6–8]. Nevertheless, the 100–300 F g^{-1} specific capacity of ACs cathode based on the physical adsorption/desorption of solvated ions at the electrolyte-electrode interface is much lower than that of anode via faradaic process, such a huge capacity difference between cathode and anode impedes the full realization of the high energy density concept [9,10]. Additionally, the energy densities of hybrid capacitors often degrade noticeably at high rates due to the differences in the charge storage kinetics between anode and cathode, because of the reaction kinetics of anode based on the faradaic reaction is far slower than that of the cathode [11,12].

The surface functional groups modification on ACs can be regarded as an alternative solution to improve the capacitance with the aid of pseudocapacitive effect. For instance, Leon L. Shaw functionalized AC powders with C=O groups, leading to the specific capacitance increasing 3 times, which lies in that Li^+ react with C=O groups reversibly to impart pseudocapacitance [13,14]. Unfortunately, the cycle stability of functionalized ACs cathode is always a concern due to the irreversible reactions between oxygen and electrolyte ions, giving rise to the decomposition of the electrolyte [15]. Moreover, the oxygen-modification can distinctly diminish the electrical conductivity of the electrode materials and consequently worsen their electrochemical performance. Recent studies have revealed that addition of lithiated

* Corresponding author.
E-mail address: wencuili@dlut.edu.cn (W.-C. Li).

https://doi.org/10.1016/j.jpowsour.2018.06.003
Received 28 January 2018; Received in revised form 5 May 2018; Accepted 1 June 2018
Available online 07 June 2018
0378-7753/

intercalation materials into the ACs cathode of lithium-ion hybrid capacitors is another possible strategy to enhance energy density [16–18]. The energy density of hybrid capacitors by using $LiCoO_2$ combined with 5%–20% ACs as cathode and nanostructured $Li_4Ti_5O_{12}$ as anode can be up to 40 Wh kg^{-1}, which is higher than that of hybrid capacitors with ACs as cathode [19]. Due to the low theoretical specific capacity (150–250 mA h g^{-1}) of lithiated intercalation materials, a large amount of materials are needed to add into the ACs cathode to achieve high energy density, while, this will result in an unsatisfied power capability [20,21]. The above unsolved problems have motivated the investigations of alternative cathodes to improve the energy density of hybrid capacitors without compromising their cyclability and power capability. On the other hand, for anode, attempts mainly focus on enhancing rate performance by shortening the ion diffusion length or using pseudocapacitive anode that can reduce the gap of kinetic imbalances during electrochemical reactions in anode and cathode electrodes to realize a high rate performance for hybrid capacitors.

Sulfur(S), a light-weight element, possesses a high theoretical capacity of 1675 mAh g^{-1} based on a two-electron transfer reaction, which is an order of magnitude higher than that of the lithiated intercalation material [22–24]. In combination with the natural abundance and environmental friendliness, sulfur is considered as the next-generation cathode materials for lithium-sulfur (Li-S) battery. Nevertheless, its practical application is hindered currently by the insulating nature of sulfur and high solubility of the long-chain lithium polysulfides generated during the discharge/charge process [25,26]. To settle these shortcomings, sulfur is always incorporated into carbon materials that are capable of delivering electrons efficiently to the sulfur as well as trapping the soluble polysulfides [27,28]. In theory, the lower sulfur content in the carbon host, the higher the sulfur utilization and cycle stability. However, in principle, high sulfur content ($\geq$70%) is required in Li-S batteries for achieving a higher energy density [29,30].

Taking another look at the high capacity and shuttle effect of electroactive sulfur at high content, and considering the demands of hybrid capacitors for cathode materials, we propose a use of highly conductive porous carbon loaded a small amount of sulfur as a cathode to well match LIB-type anode. In this situation, the small amount of sulfur filled in the pores of the carbon materials can provide high specific capacity and restrict the dissolution of polysulfides, and the problem of huge capacity difference between cathode and anode of hybrid capacitors will be overcome. Additionally, the kinetics of sulfur based on the redox reaction is similar to that of most anode materials, which narrows the kinetics gap between two electrodes and makes the cathode kinetically match well with the anode.

Herein, we reported the use of carbon-sulfur composite as the cathode to improve the energy density of hybrid capacitors. The resultant composite cathode delivered a high specific capacity of 212.2 mAh g^{-1} (424.4 F g^{-1}) at 4 A g^{-1}, much better than that of the activated carbons without sulfur. Benefiting from the high capacity and moderate kinetics of the carbon-sulfur composite cathode, the fabricated hybrid capacitors delivered a high energy density of 258.4 Wh kg^{-1} at 995 W kg^{-1} and high cycle stability over 3000 running. This result clearly indicates that the carbon-sulfur composite is a promising candidate for high energy density hybrid capacitors, which will give further impetus to explore the fundamental science and applications of sulfur in the context of electrochemical energy storage.

2. Experimental section

2.1. Materials synthesis

At first, the commercially available porous carbon (Ketjenblack EC-600JD) denoted as C-01 and sulfur were ground together, heated to 155 °C in a sealed vacuum tube with a holding time of 12 h to facilitate sulfur diffusion into the carbon host. Then, the composite was maintained in an oven at 300 °C to volatilize sulfur residue on the outer surface of the carbon host. The content of sulfur in the carbon-sulfur composites was varied to be 23 wt% and 33 wt% by adjusting the heating time at 300 °C, which were named CS-02 and CS-03, respectively. The CS-02 with 23 wt% sulfur was obtained by maintaining the carbon-sulfur composite with 70 wt% sulfur in an oven at 300 °C for 160 min and the CS-03 with 33 wt% sulfur was obtained by maintaining the carbon-sulfur composite with 70 wt% sulfur in an oven at 300 °C for 90 min.

2.2. Characterization methods

Microstructural analysis was conducted with a field emission scanning electron microscope (SEM) by using a Hitachi S-4800 instrument at 10 kV, equipped with an energy dispersive X-ray spectrometer (EDX) for detecting the elemental signals and collecting the elemental mapping signals. Nitrogen adsorption-desorption isotherms were measured with a Tristar 3000 sorption analyzer (Micromeritics) at 77.4 K. Before the measurements, the carbon sample C-01 was degassed under vacuum at 200 °C for 12 h and CS-02 and CS-03 was degassed under vacuum at 50 °C for 16 h until the pressure was less than 5 Pa. Pore size distributions were determined from the adsorption branches of the isotherms using density functional theory. The Brunauer-Emmett-Teller (BET) method was used to calculate the specific surface areas (S_{BET}). Total pore volumes were calculated from the amount adsorbed at a relative pressure, P/P_0, of 0.99. XRD patterns were obtained with a Rigaku D/MAX-2400 diffractometer using Cu Kα radiation (40 kV, 100 mA, λ = 1.54056 Å). TEM analyses were carried out with a Tecnai G220S-Twin instrument operating at 200 kV. Samples for TEM analysis were prepared by dropping an ethanol droplet of the products on carbon-coated copper grids and drying at room temperature. Thermogravimetric analysis (TGA) was measured from 40 to 800 °C with a heating rate of 10 °C min^{-1} under a nitrogen flow, using a STA449 F3 Jupiter thermogravimetric analyzer (NETZSCH). XPS data were obtained with an ESCALAB250 electron spectrometer. The conductivity of CS-02 and CS-03 were tested by four-tip probes method.

2.3. Electrochemical characterization

2.3.1. Preparation of electrodes

The cathodes were fabricated by mixing 75 wt% C-01, CS-02 or CS-03 with 15 wt% conductive carbon black and 10 wt% PVDF binder. The anode was prepared by using a mixture of 80 wt% commercial hard carbon, 10 wt% CNT conductive additives, and 10 wt% binder (LA133 and CMC). The mass loadings of the active materials in both cathode and anode are about 1–1.2 and 1.5–2 mg cm^{-2}, respectively.

2.3.2. Assembly of half-cells and LICs

Half cells were assembled to measure the electrochemical performances of C-01, CS-02, CS-03 and commercial hard carbon, in which lithium metal foil was used as the counter and reference electrode and 1 M LiTFSI in DME/DOL (1:1, v/v) was employed as the electrolyte. Celgard 2400 was used as a separator. Commercial hard carbon (HC) electrode was pre-activated for 3 cycles at 50 mA g^{-1} in a Li half-cell to obtain high efficiency and then lithiated to 0.05 V, and then the pre-activated HC anode was coupled with a CS-02 cathode to fabricate a hybrid capacitors, and the mass ratio of cathode/anode was 1:1.5.

2.3.3. Electrochemical tests

Galvanostatic charge/discharge tests of half cells were conducted in a voltage window of 1.7–3.5 V for C-01, CS-02 and CS-03 and 0.01–2.8 V for HC by using a LAND-CT2001 instrument at a room temperature. The specific capacity of the cathode was calculated based on the total mass of sulfur and carbon. Cyclic voltammetry (CV), galvanostatic charge/discharge cycling (GC) and electrochemical impedance spectroscopy (EIS) of hybrid capacitors were performed on a CHI660D electrochemical workstation (CH Instruments, China).

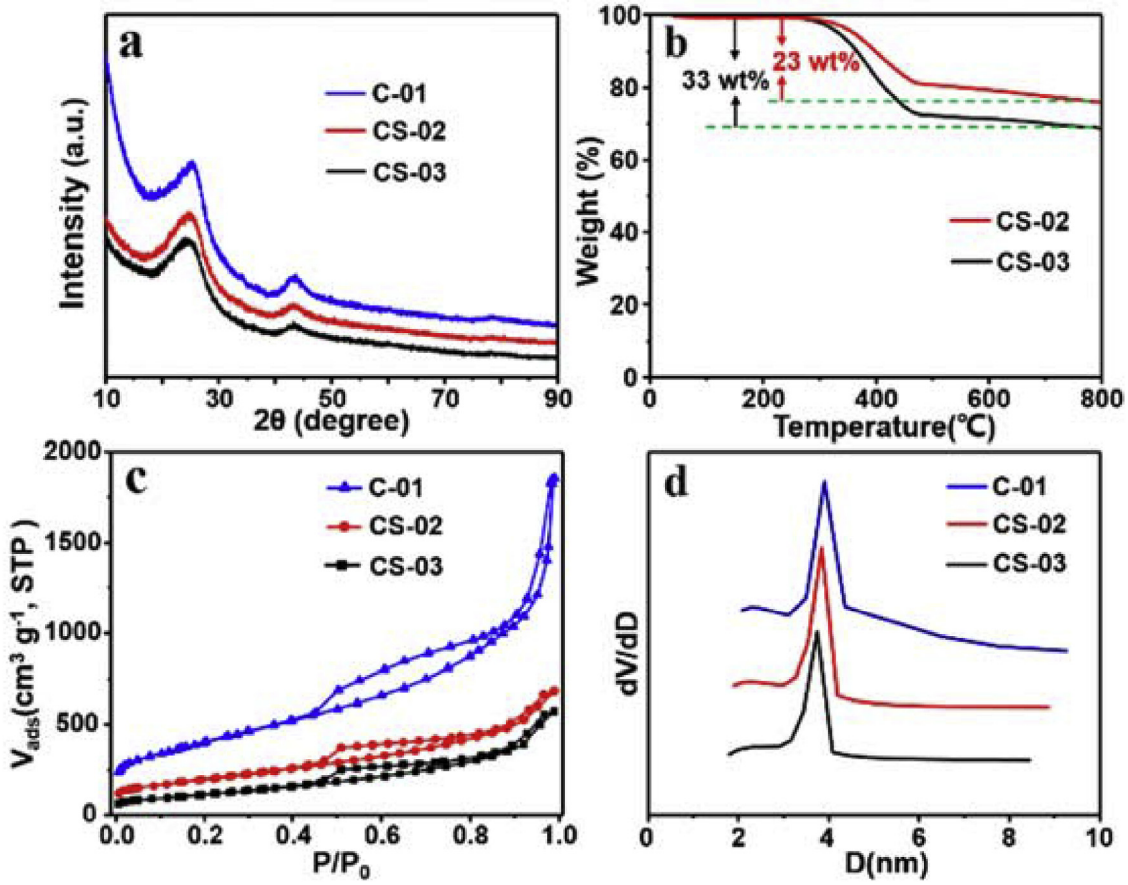

Fig. 1. (a) XRD patterns of C-01, CS-02 and CS-03; (b) TGA curves of CS-02 and CS-03; (c) N_2 adsorption-desorption isotherms of C-01, CS-02 and CS-03; (d) Pore size distributions of C-01, CS-02 and CS-03.

Stability measurements of the hybrid capacitors were carried out using a Land CT2001A battery test system.

3. Results and discussion

Commercially available Ketjenblack EC-600JD (denoted as C-01) was used as the host material for sulfur infiltration due to its high surface area (1400 $m^2 g^{-1}$) and high conductivity (~10000 $S m^{-1}$), which can enable a uniform distribution of sulfur in the carbon and facilitate electron transport within the carbon-sulfur composite. The carbon-sulfur composites CS-02 and CS-03 were prepared by varying sulfur content as 23 wt% and 33 wt%, respectively. The absence of peaks corresponding to bulk crystalline sulfur in XRD patterns of CS-02 and CS-03 (Fig. 1a) demonstrates that the sulfur is well confined and dispersed in the carbon structure [31,32]. As determined by TGA, the sulfur content in the CS-02 and CS-03 is 23 wt% and 33 wt%, respectively (Fig. 1b). Additionally, the CS-02 displays a delayed sulfur vaporization temperature (~320 °C) compared to CS-03 (~300 °C) and most reported carbon-sulfur composite (200–300 °C) [33,34], indicating the lower content of sulfur, the better confined effect in the pore channels. In this case, the diffusion of polysulfide will be alleviated [35]. The introduction of small amount of sulfur essentially does not change the type-IV features of the nitrogen sorption isotherm of carbon material C-01 (Fig. 1c), indicating the mesoporous structure is maintained, which potentially facilitates the transport of electrolyte and improves the rate performance. The sample CS-02 and CS-03 still have high specific surface area and pore volume of (610 $m^2 g^{-1}$, 1.02 $cm^3 g^{-1}$) and (425 $m^2 g^{-1}$, 0.89 $cm^3 g^{-1}$), respectively. Fig. 1d shows that the pore size slightly narrows down after the sulfur filling, indicating that sulfur was stored in the pore channels, which is consistent with the results of XRD and TGA. Although the carbon loaded with 23 wt% non-conducting sulfur, the conductivity of CS-02 still reaches up to ~3000 $S m^{-1}$ determined by a 4-point probe measurement, which is much higher than those of carbon black such as Vulcan XC-72 carbon (150 $S m^{-1}$) [36]. The sample CS-03 has lower conductivity of ~2270 $S m^{-1}$ due to its higher sulfur content.

As a representative sample, CS-02 was further characterized by SEM and TEM. CS-02 is composed of interconnected carbon particles and no visible large sulfur agglomerations are observed (Fig. 2a). TEM image shows that the carbon particles with high graphitization degree (insert in Fig. 2b) are interconnected to form a conductive network and no any large sulfur particles are observed (Fig. 2b) in the composite, indicating a high dispersity of sulfur in the carbon. The elemental mappings of carbon and sulfur for CS-02 (Fig. 2c–e) clearly show that carbon and sulfur are distributed uniformly in the composite, further confirming the high dispersity.

The electrochemical performances of carbon-sulfur composites were initially evaluated by using a Li half-cell in a voltage window of 1.7–3.5 V (Figure S1). The cyclic voltammograms (CVs) of CS-02 cathode (Fig. 3a) at the potential below 2.75 V is quite similar to that of carbon-sulfur electrodes in lithium-sulfur batteries, showing two cathodic peaks at ca. 2.35 and 1.90 V (versus Li^+/Li) due to the two-step reduction of sulfur to polysulfides [37,38]. While the oxidation peak at ca. 2.45 V corresponds to the reverse reactions of polysulfide back to the sulfur. The sharp redox peaks of CS-02 indicate the fast kinetics during the reversible electrochemistry reaction [39]. Furthermore, as the sweep rate increases to 1.8 mV s^{-1}, the shape of CV curves is still retained, suggesting small polarization of the electrode at high rates [12]. It is worth pointing out that the quasi-rectangular shape at 2.75–3.50 V (the insert in Fig. 3a) corresponds to a non-faradaic

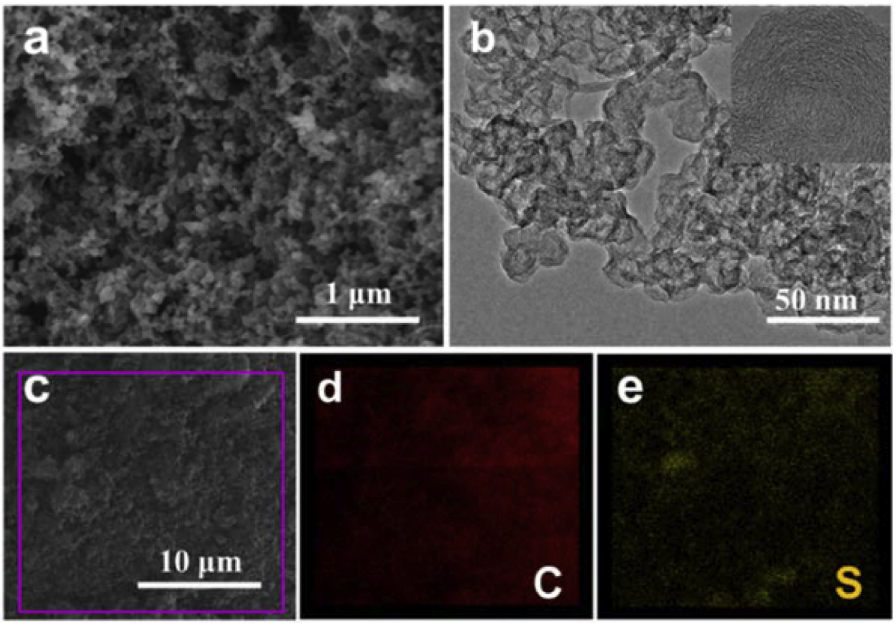

Fig. 2. (a) SEM and (b) TEM of the CS-02; (c-e) element mapping of the carbon and sulfur.

reaction, reflecting energy-storage mechanism in the sample CS-02 resulted from the co-contribution of faradaic and non-faradaic reactions [40]. In order to study the contribution from the capacitive behavior, Trasatti procedure was conducted to quantify the charge storage from the easily accessible outer surface and the not easily accessible inner surface (see the supporting information) [8]. The contribution ratios of the inner and outer charge process at different scan rates are shown in Fig. 3b. The outer charge contribution gradually improves with the increases of scan rate. Figure S2 shows typical galvanostatic charge/discharge curves at 0.5 A g^{-1} within a voltage window of 1.7–3.5 V.

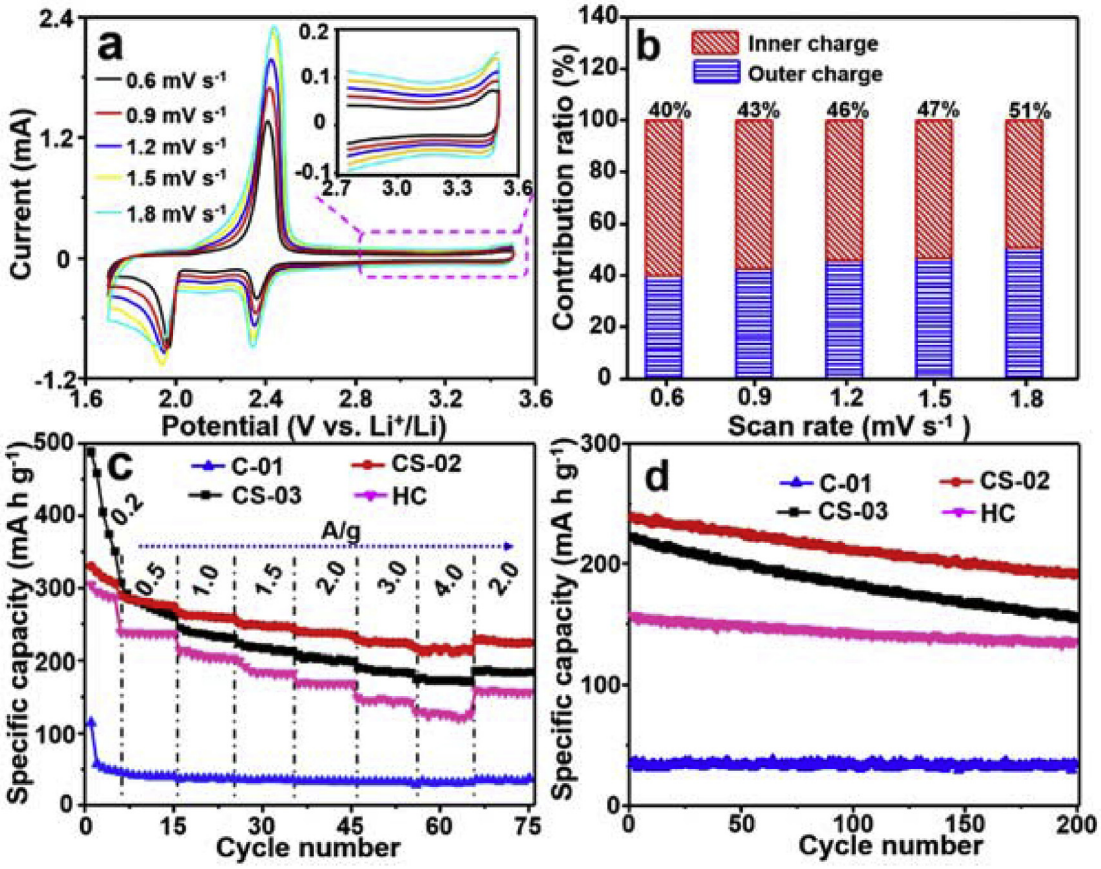

Fig. 3. (a) CV curve of CS-02 at different scan rates. (b) Contribution ratio of the inner and outer charge storage of CS-02 at different scan rates. (c) Rate performances of C-01, CS-02, CS-03 and HC. (d) Cycling performances of C-01, CS-02, CS-03 and HC at 2 A g^{-1}.

The discharge and charge profiles clearly show two plateaus, which are consistent with the CV results.

Fig. 3c shows the CS-2 electrode exhibiting the best rate performance. A high specific capacity of 280.7 mAh g^{-1} (561.4 F g^{-1}) at 0.5 A g^{-1} can be obtained based on the total mass of carbon-sulfur composite. Even at a high current density of 4 A g^{-1}, ca. 212.2 mAh g^{-1} (424.4 F g^{-1}) discharge capacity is maintained, corresponding to a capacity retention of 75.5% when the rate is increased 8-fold. Moreover, when the current density is set back to 2 A g^{-1} after cycling at different rates, the specific capacity can be recovered to 228.3 mAh g^{-1}, indicating very stable cycling performance. For CS-03, due to the fact that the low conductivity of the carbon-sulfur composite leads to low sulfur utilization, it shows poor rate performance. Although the sample C-01 without sulfur loading shows the highest capacity retention (77.6%) from 0.5 A g^{-1} to 4 A g^{-1}, it shows very low specific capacity. These results suggest that the CS-02 composite has an excellent rate capability, which is clearly superior to those of most reported cathodes for hybrid capacitors [3,6]. The commercial hard carbon (HC) was selected as the anode electrode material due to its high specific capacity and high cycling stability at high rates [41,42]. It delivers a rate capacity of ca. 237.6 mAh g^{-1} at 0.5 A g^{-1} (Fig. 3c). Even at a high current density of 4 A g^{-1}, the specific capacity can reach 126.7 mAh g^{-1}, corresponding to a capacity retention of about 53.3%. Moreover, when the current density is switched abruptly from 4 to 2 A g^{-1} again, the capacity is largely recovered to 157.2 mAh g^{-1}, indicating unexceptionable stability of the anode materials. Note that the capacity retention from 0.5 A g^{-1} to 4 A g^{-1} of CS-02 cathode is lower than the C-01 cathode but higher than the anode, which means that the reaction kinetics of CS-02 cathode is slower than the C-01 but still faster than anode. In this case, the kinetics gap between cathode and anode is narrowed by using CS-02 as cathode, making the cathode match well with the anode. Benefiting from low sulfur content and the confinement of sulfur in the carbon host with high conductivity and high specific surface area, the CS-02 (Fig. 3d) also shows favorable cycling stability with an initial capacity of 238.5 mAh g^{-1} and a capacity retention of 80.9% after 200 cycles at 2 A g^{-1}. The CV curves of CS-02 at different cycles (Figure S3) exhibit sharper anodic/cathodic peaks with nearly-overlapped form, indicating the high reversibility and cycling stability of CS-02. Although the sample C-01 has better stability, the capacity is very low. The sample HC also exhibits favorable cycling behavior at 2 A g^{-1}, delivering an initial capacity of 156.0 mAh g^{-1} and a capacity retention of 86.8% after 200 cycles. Based on the excellent electrochemical properties, CS-02 was chosen as the cathode material for the subsequently fabricated hybrid capacitor.

The electrochemical performances of hybrid capacitors, which were assembled using CS-02 as the cathode material and HC as the anode material, are shown in Fig. 4. Different from the symmetric supercapacitor with rectangular CV shape, HC//CS-02 hybrid capacitor (Fig. 4a) shows a deviation from the ideal rectangular shape due to the synergistic effect of two different energy-storage mechanisms. As the sweep rate increases to 200 mV s^{-1}, the shape of CV curve is still retained, demonstrating high reversibility and good rate capability. The charge and discharge profiles under different currents (Fig. 4b and Figure S5a) show deviation from the ideal capacitor, which is well matched the CV curves and again indicated that the energy-storage mechanisms in the device are resulted from the synergistic effect of faradaic and non-faradaic reactions. It is should be noted that the energy-storage mechanisms in the HC//CS-02 hybrid capacitors are different from that of the lithium-sulfur battery used hard carbon material as negative electrode [43,44] (see table S1). Moreover, the small IR drops (Fig. 4b) indicate the good rate performance of both the anode and cathode materials. The rate performances of HC//CS-02 hybrid capacitor was investigated by cycling at various current rates from 0.5 to 5.0 A g^{-1} (Figure S4). A high specific capacity of 128.9 mAh g^{-1} at 0.5 A g^{-1} can be obtained. Even at a high current density of 5 A g^{-1}, ca.93.7 mAh g^{-1} discharge capacity is maintained, corresponding to a capacity retention of 72.7% when the rate is increased 10-fold. The energy density and power density are calculated by using the charge-discharge results based on the total mass of active materials in both the cathode and anode. The HC//CS-02 hybrid capacitor (Figure S5b) shows a high energy density of 258.4 Wh kg^{-1} at 995 W kg^{-1}, which also remains at 125.3 Wh kg^{-1} even when the power density is elevated to 17350 W kg^{-1}. In contrast, the HC//C-01 hybrid capacitor (Figure S5d) shows a low energy density of 37.9 Wh kg^{-1} even when the power density is elevated to 969 W kg^{-1}. Table S2 lists some hybrid capacitors with typical energy and power densities for an approximate comparison, such as AC//hard carbon [45], AC//LTO [46], AC//B-Si/SiO_2/C [47], AC//Mn_3O_4-G [48], graphene//Fe_3O_4/graphene [49], MOF-NC//WO_3/C [50], AC//Graphitic carbon [51]. The performance in this work exhibits both better energy and power densities, which confirms that improving the specific capacity of cathode materials is essential to fully realize the high energy density concept in current hybrid capacitors.

Fig. 4c presents the cycle performance of the HC//CS-02 hybrid capacitors at a current density of 5 A g^{-1}. It is shown that 79% capacitance retains after 3000 cycles and the degradation rate is only 0.007% per cycle, indicating that the HC//CS-02 hybrid capacitor exhibits a high cycling stability. The main reason related to the drop in the capacity retention of the full cell with the number of cycles is maybe that the polysulfide generated during the cycle will partially dissolve into the electrolyte. The separator from the HC//CS-02 and HC//CS-03 cells after 500 cycles exhibit a color of polysulfide (Figure S6), while the separator from the HC//CS-02 shows a slighter coloring, indicating the lower content of sulfur, the better confined effect in the pore channels. The electrochemical impedance spectroscopy (EIS) was used to characterize the HC//CS-02 hybrid capacitor after 1000 and 1500 cycles (Figure S5e,f). As expected, both spectra show a semicircle and an inclined line at low and high frequency regions, respectively. The semicircles in the low frequency region are broad and depressed, due to the overlap of the two separate semicircles [52]. The HC//CS-02 hybrid capacitor after 1000 and 1500 cycles still has low R_s and R_{ct} value (8.2 Ω, 5.3 Ω) and (13.6 Ω, 5.3 Ω) respectively, revealing a relatively low resistance even after long cycles. It is worth mentioning that the cell with low R_{ct} value would have exhibited excellent electrochemical capacitive performance. The good electrochemical performance in this work including high energy and power density with outstanding stability should be due to the following aspects: First, the porous carbon with high electron conductivity and high surface area can facilitate the charge/ion transfer. Second, the small amount of sulfur can be confined in the pores of the carbon, which can prevent the dissolution of polysulfide during cycling, and thus improve the cycling stability. Finally, the sulfur has high theoretical capacity and nanosize, which can improve the capacity of cathode significantly, and thus make the specific capacity and kinetics of cathode match well with that of anode, improving the energy density of hybrid capacitor.

4. Conclusion

In summary, we demonstrate the concept of the carbon-sulfur composite as cathode material for the fabrication of high energy hybrid capacitor. The as-obtained carbon-sulfur composite integrate many structural merits for electrochemical process, including well-confined and homogeneously distributed sulfur, interconnected conductive framework with large surface area, which synergically enable the fabricated cathode material with an impressive reversible capacity and excellent rate capability, much better than that of pure carbon cathode. Benefiting from the high capacity of the cathode, the hybrid capacitor (HC//CS-02) assembled by using the carbon-sulfur cathode can reach a high energy density of 258.4 Wh kg^{-1} at 995 W kg^{-1}. Even at high power density of 17350 W kg^{-1}, the energy density can still remain 125.3 Wh kg^{-1}. The encouraging results presented here demonstrate that hybrid capacitor based on carbon-sulfur composites could be promising energy storage systems affording both high energy and power

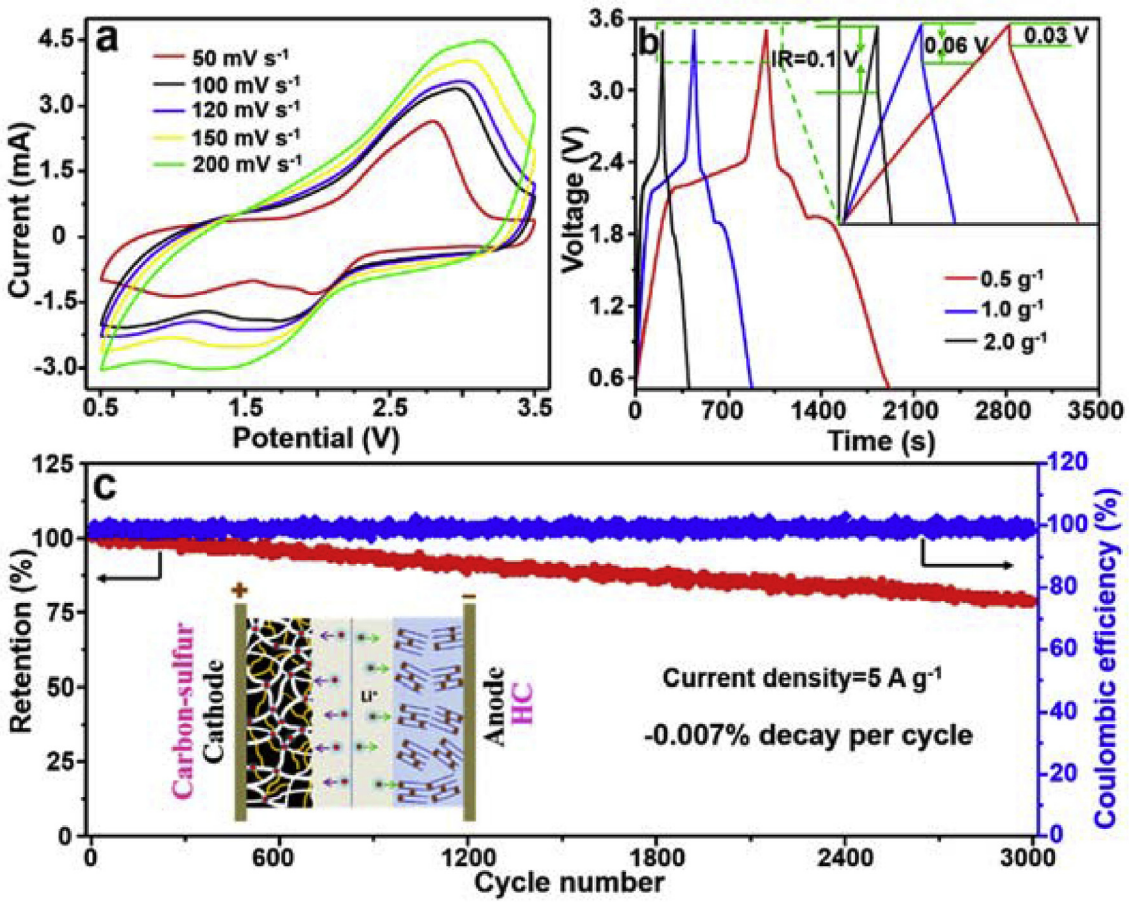

Fig. 4. (a) CV curves; (b) GC curves; (c) cycling performance and coulombic efficiency, schematic illustration of the assembled structure (the insert) of HC//CS-02.

densities.

Conflicts of interest

There are no conflicts of interest to declare.

Acknowledgements

The authors are grateful to the financial support by the National Science Fund for National Natural Science Foundation of China (No.21376047, No.21776041), and Cheung Kong Scholars Programme of China (T2015036).

Appendix A. Supplementary data

Supplementary data related to this article can be found at http://dx.doi.org/10.1016/j.jpowsour.2018.06.003.

References

[1] M. Armand, J.M. Tarascon, Nature 451 (2008) 652–657.
[2] J. Luo, W. Zhang, H. Yuan, C. Jin, L. Zhang, H. Huang, C. Liang, Y. Xia, J. Zhang, Y. Gan, X. Tao, ACS Nano 11 (2017) 2459–2469.
[3] M. Yang, Y. Zhong, J. Ren, X. Zhou, J. Wei, Z. Zhou, Adv. Energy Mater 5 (2015) 1500550.
[4] W-H. Qu, F. Han, A.-H. Lu, C. Xing, M. Qiao, W.-C. Li, J. Mater. Chem. A 2 (2014) 6549–6557.
[5] V. Aravindan, D. Mhamane, W.C. Ling, S. Ogale, S. Madhavi, ChemSusChem 6 (2013) 1–5.
[6] B. Li, F. Dai, Q. Xiao, L. Yang, J. Shen, C. Zhang, M. Cai, Energy Environ. Sci. 9 (2016) 102–106.
[7] L.L. Zhang, X.S. Zhao, Chem. Soc. Rev. 38 (2009) 2520–2531.
[8] S. Li, J. Chen, M. Cui, G. Cai, J. Wang, P. Cui, X. Gong, P.S. Lee, Small 13 (2017) 1602893.
[9] X. Yu, C. Zhan, R. Lv, Y. Bai, Y. Lin, Z.H. Huang, W. Shen, X. Qiu, F. Kang, Nano Energy 15 (2015) 43–53.
[10] Z. Shi, J. Zhang, J. Wang, J. Shi, C. Wang, Electrochim. Acta 153 (2015) 476–483.
[11] H. Wang, Y. Zhang, H. Ang, Y. Zhang, H.T. Tan, Y. Zhang, Y. Guo, J.B. Franklin, X.L. Wu, M. Srinivasan, H.J. Fan, Q. Yan, Adv. Funct. Mater. 26 (2016) 3082–3093.
[12] L. Shen, H. Lv, S. Chen, P. Kopold, P.A. Aken, X. Wu, J. Maier, Y. Yu, Adv. Mater. (2017) 1700142.
[13] C. Liu, B.B. Koyyalamudi, L. Li, S. Emani, C. Wang, L.L. Shaw, Carbon 109 (2016) 163–172.
[14] S.K. Park, Q. Mahmood, H.S. Park, Nanoscale 5 (2013) 12304–12309.
[15] Q. Wang, J. Yan, Z. Fan, Energy Environ. Sci. 9 (2016) 729–762.
[16] D. Ruan, Y. Huang, L. Li, J. Yuan, Z. Qiao, J. Alloy. Comp. 695 (2017) 1685–1690.
[17] K. Karthikeyan, S. Amaresh, K.J. Kim, S.H. Kim, K.Y. Chung, B.W. Cho, Y.S. Lee, Nanoscale 5 (2013) 5958–5964.
[18] M. Secchiaroli, G. Giuli, B. Fuchs, R. Marassi, M. Wohlfahrt-Mehrensa, S. Dsoke, J. Mater. Chem. A 3 (2015) 11807–11816.
[19] A.D. Pasquier, I. Plitz, J. Gural, F. Badway, G.G. Amatucci, J. Power Sources 136 (2004) 160–170.
[20] V. Aravindan, J. Gnanaraj, Y.S. Lee, S. Madhavi, Chem. Rev. 114 (2014) 11619–11635.
[21] F. Cheng, S. Wang, A.-H. Lu, W.-C. Li, J. Power Sources 229 (2013) 249–257.
[22] B. He, W.-C. Li, C. Yang, S.Q. Wang, A.-H. Lu, ACS Nano 10 (2016) 1633–1639.
[23] Q. Sun, B. He, X.-Q. Zhang, A.-H. Lu, ACS Nano 9 (2015) 8504–8513.
[24] S. Yuan, Z. Guo, L. Wang, S. Hu, Y. Wang, Y. Xia, Adv. Sci. 2 (2015) 1500071.
[25] Y. Zhao, M. Liu, W. Lv, Y.-B. He, C. Wang, Q. Yun, B. Li, F. Kang, Q.-H. Yang, Nanomater. Energy 30 (2016) 1–8.
[26] Y.X. Yin, S. Xin, Y.-G. Guo, L.-J. Wan, Angew. Chem. Int. Ed. 52 (2013) 2–18.
[27] L.H. Zhang, B. He, W.-C. Li, A.-H. Lu, Adv. Energy Mater (2017) 1701518.
[28] S. Chen, B. Sun, X. Xie, A.K. Mondal, X. Huang, G. Wang, Nano Energy 16 (2015) 268–280.
[29] L. Miao, W. Wang, K. Yuan, Y. Yang, A. Wang, Chem. Commun. 50 (2014) 13231–13234.
[30] R. Fang, S. Zhao, Z. Sun, D.W. Wang, H.M. Cheng, F. Li, Adv. Mater. (2017) 1606823.
[31] J.S. Lee, W. Kim, J. Jang, A. Manthiram, Adv. Energy Mater. (2016) 1601943.
[32] H. Chen, C. Wang, W. Dong, W. Lu, Z. Du, L. Chen, Nano Lett. 15 (2015) 798–802.
[33] D. Li, F. Han, S. Wang, F. Cheng, Q. Sun, W.-C. Li, ACS Appl. Mater. Interfaces 5 (2013) 2208–2213.
[34] D. Su, M. Cortie, G. Wang, Adv. Energy Mater. (2017) 1602014.

[35] J.T. Lee, Y. Zhao, S. Thieme, H. Kim, M. Oschatz, L. Borchardt, A. Magasinski, W. Cho, S. Kaskel, G. Yushin, Adv. Mater. 25 (2013) 4573–4579.
[36] Z. Cui, C. Zu, W. Zhou, A. Manthiram, J.B. Goodenough, Adv. Mater. 28 (2016) 6926–6931.
[37] J. Liu, W. Li, L. Duan, X. Li, L. Ji, Z. Geng, K. Huang, L. Lu, L. Zhou, Z. Liu, W. Chen, L. Liu, S. Feng, Y. Zhang, Nano Lett. 15 (2015) 5137–5142.
[38] J. He, Y. Chen, P. Li, F. Fu, Z. Wang, W. Zhang, J. Mater. Chem. A 3 (2015) 18605–18610.
[39] G.C. Li, G.R. Li, S.H. Ye, X.P. Gao, Adv. Energy Mater 2 (2012) 1238–1245.
[40] P. Shang, J. Zhang, W. Tang, Q. Xu, S. Guo, Adv. Funct. Mater. 26 (2016) 7766–7774.
[41] H. Yu, X. Dong, Y. Pang, Y. Wang, Y. Xia, Electrochim. Acta 228 (2017) 251–258.
[42] X. Sun, X. Zhang, H. Zhang, N. Xu, K. Wang, Y. Ma, J. Power Sources 270 (2014) 318–325.
[43] S. Thieme, J. Bruckner, A. Meier, I. Bauer, K. Gruber, J. Kaspar, A. Helmer, H. Althues, M. Schmuck, S. Kaskel, J. Mater. Chem. A 3 (2015) 3808–3820.
[44] J. Brückner, S. Thieme, F. Böttger-Hiller, I. Bauer, H.T. Grossmann, P. Strubel, H. Althues, S. Spange, S. Kaskel, Adv. Funct. Mater. 24 (2014) 1284–1289.
[45] J.H. Kim, J.S. Kim, Y.G. Lim, J.G. Lee, Y.J. Kim, J. Power Sources 196 (2011) 10490–10495.
[46] A. Jain, V. Aravindan, S. Jayaraman, P.S. Kumar, R. Balasubramanian, S. Ramakrishna, S. Madhavi, M.P. Srinivasan, Sci. Rep. 3 (2013) 3002.
[47] R. Yi, S. Chen, J. Song, M.L. Gordin, A. Manivannan, D. Wang, Adv. Funct. Mater. 24 (2014) 7433–7439.
[48] M. Ulaganathan, V. Aravindan, W.C. Ling, Q. Yan, S. Madhavi, J. Mater. Chem. A 4 (2016) 15134–15139.
[49] F. Zhang, T. Zhang, X. Yang, L. Zhang, K. Leng, Y. Huang, Y. Chen, Energy Environ. Sci. 6 (2013) 1623–1632.
[50] J. Xu, Y. Li, L. Wang, Q. Cai, Q. Li, B. Gao, X. Zhang, K. Huo, P.K. Chu, Nanoscale 8 (2016) 16761–16768.
[51] Z. Yang, H. Guo, X. Li, Z. Wang, Z. Wang, Y. Wang, Z. Yan, D. Zhang, J. Mater. Chem. A 5 (2017) 15302–15309.
[52] K. Kaliyappan, S. Amaresh, Y.S. Lee, ACS Appl. Mater. Interfaces 6 (2014) 11357–11367.